Original Article | Gastrointestinal Imaging

eISSN 2005-8330
https://doi.org/10.3348/kjr.2021.0451
Korean J Radiol 2022;23(2):189-201

Korean Journal of Radiology
KJR

Ablative Outcomes of Various Energy Modes for No-Touch and Peripheral Tumor-Puncturing Radiofrequency Ablation: An *Ex Vivo* Simulation Study

Dong Ik Cha[1], Min Woo Lee[1, 2], Kyoung Doo Song[1, 2], Seong Eun Ko[1], Hyunchul Rhim[1, 2]

[1]Department of Radiology and Center for Imaging Science, Samsung Medical Center, Sungkyunkwan University School of Medicine, Seoul, Korea; [2]Department of Health Sciences and Technology, SAIHST, Sungkyunkwan University, Seoul, Korea

Objective: To compare the outcomes of radiofrequency ablation (RFA) using dual switching monopolar (DSM), switching bipolar (SB), and combined DSM + SB modes at two different interelectrode distances (25 and 20 mm) in an *ex vivo* study, which simulated ablation of a 2.5-cm virtual hepatic tumor.

Materials and Methods: A total of 132 ablation zones were created (22 ablation zones for each protocol) using three separable clustered electrodes. The performances of the DSM, SB, and combined DSM + SB ablation modes were compared by evaluating the following parameters of the RFA zones at two interelectrode distances: shape (circularity), size (diameter and volume), peritumoral ablative margins, and percentages of the white zone at the midpoint of the two electrodes (ablative margin at midpoint, AMm) and in the electrode path (ablative margin at electrode path, AMe).

Results: At both distances, circularity was the highest in the SB mode, followed by the DSM + SB mode, and was the lowest in the DSM mode. The circularity of the ablation zone showed a significant difference among the three energy groups ($p < 0.001$ and $p = 0.002$ for 25-mm and 20-mm, respectively). All size measurements, AMm, and AMe were the greatest in the DSM mode, followed by the DSM + SB mode, and the lowest were with the SB mode (all statistically significant). The white zone proportion in AMm and AMe were the greatest in the SB mode, followed by the DSM + SB mode and DSM in general.

Conclusion: DSM and SB appear to be complementary in creating an ideal ablation zone. RFA with the SB mode can efficiently eradicate tumors and create a circular ablation zone, while DSM is required to create a sufficient ablative margin and a large ablation zone.

Keywords: *Radiofrequency ablation; Electrodes; Liver; Animal experimentation*

INTRODUCTION

Radiofrequency ablation (RFA) is a widely used ablative modality for treating hepatocellular carcinoma (HCC). The conventional RFA method involves inserting a single, monopolar, internally cooled electrode tip into a tumor. Multiple overlapping ablations may be performed to ablate the tumor and the surrounding liver parenchyma [1,2]. However, the ideal repositioning of the electrode is sometimes technically challenging; hence, an overlapping ablation may still result in a non-spherical ablation zone and an insufficient ablative margin [3,4]. Therefore, local tumor progression (LTP) rates after conventional monopolar RFA have been reported to be as high as 27% at 5 years [5].

Meanwhile, multipolar RFA using multiple electrodes with the no-touch technique, wherein two or more electrodes are inserted outside the index tumor, can create a larger ablation zone than conventional tumor-puncturing monopolar ablation, while also achieving a greater ablative margin. Therefore, multipolar RFA for HCC treatment has been reported to achieve more complete pathologic necrosis, better primary RFA success, and sustained local

Received: June 3, 2021 **Revised:** August 13, 2021
Accepted: September 13, 2021
Corresponding author: Min Woo Lee, MD, Department of Radiology and Center for Imaging Science, Samsung Medical Center, Sungkyunkwan University School of Medicine, 81 Irwon-ro, Gangnam-gu, Seoul 06351, Korea.
• E-mail: leeminwoo0@gmail.com

tumor response [6-8].

There have been considerable advances in RF energy delivery systems. Switching bipolar (SB) ablation is capable of inducing more efficient necrosis between electrodes than monopolar ablation [9]. Dual switching monopolar (DSM) ablation is capable of producing a larger ablation volume than consecutive/switching monopolar ablation [10]. However, the ablative performance of the combined DSM + SB energy mode has not been reported thoroughly. Understanding the properties of various RFA energy modes and the resultant ablation zone geometry will enable a more successful procedure when using multiple electrodes.

Therefore, this study aimed to evaluate the shape, size, and ablative margins of the RFA zone using multiple electrodes under the DSM, SB, and DSM + SB energy modes at two interelectrode distances (25 and 20 mm) in an *ex vivo* study, which simulated ablation of a 2.5-cm virtual hepatic tumor.

MATERIALS AND METHODS

Ex Vivo Experimental Setting

RFA was performed on freshly explanted bovine liver tissue. The livers were placed in a tank filled with saline at room temperature (Fig. 1A). The ground pads for the monopolar mode were attached to the sides of the tank. The electrodes were inserted into the liver in a triangular array using a Y-shaped jig with multiple holes (at 5-mm intervals) at each arm to ensure a constant distance between the electrodes (Fig. 1B). Three electrodes were inserted into the liver at a depth of approximately 4–5 cm.

Radiofrequency Ablation Protocol

A multichannel RF system (VIVA Multi RF Generator, Starmed) was used, capable of both monopolar and bipolar energy modes and automatic switching of RF energy according to impedance changes (Fig. 2).

We used a separable, 15-gauge, clustered electrode (Octopus® electrode; STARmed) with three internally cooled electrodes, each with a 2.5-cm long exposed tip. The electrode tip temperature was kept below 25°C by infusing normal saline at 0°C into the lumen of each electrode using a peristaltic pump (VIVA Pump; STARmed).

This study assumed the ablation of a 2.5-cm-diameter virtual tumor because this size seemed to be appropriate for evaluating the ablation performance of various energy modes of RFA. The interelectrode distance may be too close for smaller tumors and thus may not show significant differences in ablative outcomes among energy modes. Meanwhile, it is challenging to lead to a successful no-touch RFA if the tumor is larger than 2.5-cm. A recent multicenter clinical trial also showed that no-touch RFA was safe and effective for 2.5-cm or smaller HCC [11]. According to calculations, an interelectrode distance of approximately 25 mm would enable no-touch ablation, whereas a distance of approximately 20 mm would enable peripheral tumor-puncturing ablation (Fig. 3A). Peripheral tumor-puncturing ablation was considered in this study because strict no-touch ablation is sometimes difficult to achieve; unavoidable or unintended peripheral puncturing of a tumor may occur while attempting no-touch ablation [6].

Three protocols (DSM, SB, and DSM + SB), according to the energy modes used, were applied for each interelectrode distance. As a large ablation zone can be created quickly

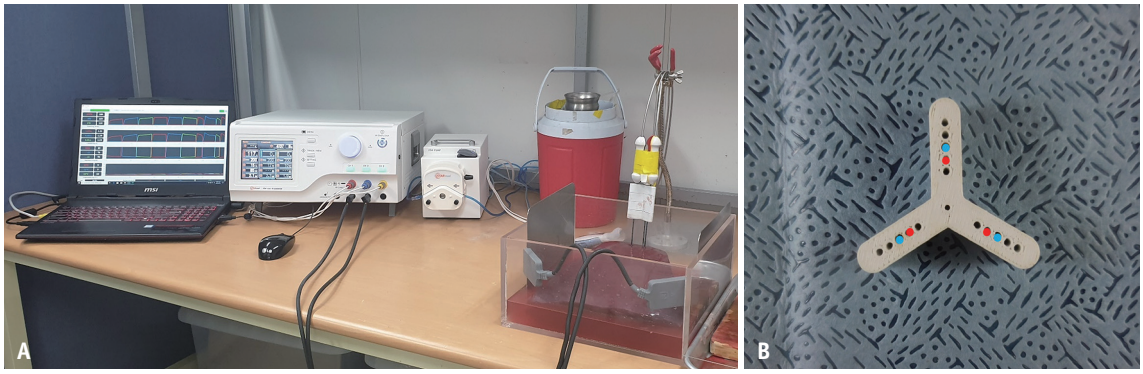

Fig. 1. The *ex vivo* experimental setting for radiofrequency ablation.
A. The explanted bovine livers were placed in a tank filled with saline at room temperature. The ground pads for the monopolar ablation mode were attached to the sides of the water tank. Three electrodes were inserted into the liver at a depth of approximately 4–5 cm. **B.** The electrodes were inserted into the liver in a triangular array at an interelectrode distance of 25 mm (blue dots) or 20 mm (red dots) using a Y-shaped jig with multiple holes in each arm to ensure a constant distance between the electrodes.

https://doi.org/10.3348/kjr.2021.0451

Korean Journal of Radiology
KJR

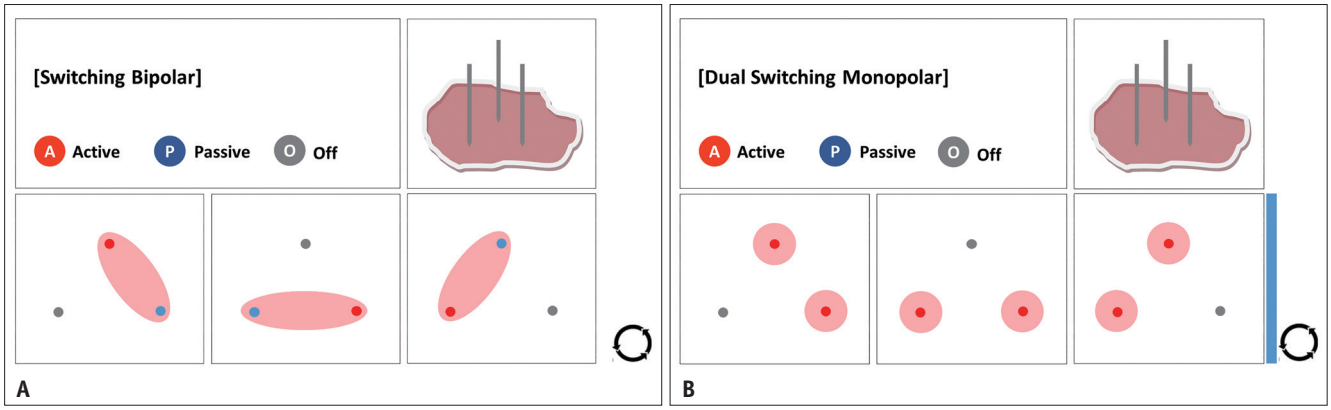

Fig. 2. Schematic showing the SB and DSM energy modes for radiofrequency ablation.
A. In the SB mode, a pair of electrodes, active and passive, are turned on. The current flows from the active electrode to the passive electrode, and ablation occurs between the two electrodes. The energy delivery switches to another pair when the impedance of the electrode increases. **B.** In DSM mode, a pair of electrodes, both of which are active, are turned on. The current flows from the two active electrodes to the passive ground pad (blue) attached to the liver. Ablation occurs around each of the two electrodes and merges to form the final ablation zone. When the impedance of one of the electrodes increased, the energy delivery switched automatically to the other electrode. DSM = dual switching monopolar, SB = switching bipolar

with multiple electrodes, the total ablation time for each protocol was 5 minutes. For the DSM + SB mode, 2 minutes of DSM and 3 minutes of SB were applied accordingly. The maximum RF energy (200 W) was delivered to a pair of electrodes during ablation from the beginning, which was then automatically switched to another pair when the tissue impedance increased above the threshold. The total energy delivered during the ablation was recorded.

Preparation of Cut Planes of the Ablation Zone

After ablation, the bovine liver blocks were cut parallel to the electrode tracts. This cut was made in the longitudinal plane to include one of the electrode tracts and the midline between the other two electrodes. Thereafter, a second cut was made in a transverse plane perpendicular to the electrode tracks so that the cut plane traversed the center of the ablation zone (Fig. 4A).

General Outcomes of RFA

All cut planes were first photographed alongside a ruler; the measurements were subsequently performed using Image J software (https://imagej.nih.gov) to prevent any bias and errors.

Since tissue contraction occurs after ablation, it was presumed that the actual interelectrode distance after ablation would be smaller than the original interelectrode distance at the time of electrode placement. Therefore, the actual interelectrode distance after ablation was measured, and the contraction rate was calculated using the changes in the electrode distance (Fig. 3B). The calculated contracted virtual tumor was drawn over the actual ablation zone to evaluate whether it fitted well for no-touch ablation at a 25-mm interelectrode distance (Fig. 3C) and peripheral tumor-puncturing ablation at a 20-mm interelectrode distance (Fig. 3D).

The circularity of the ablation zone on the second transverse cut plane was automatically calculated by drawing a region of interest along the outer margin of the ablation zone using Image J software. Circularity was defined as follows:

$$C = 4\pi A/P^2$$

where A is the area of the measured zone and P is the perimeter of the area [12].

Size Outcomes of RFA

The maximum (Dmax) and minimum (Dmin) diameters were measured from the transverse cut plane (Fig. 4B, C). The longest vertical diameter (Dv) parallel to the electrode path was measured in the longitudinal plane (Fig. 4D). The volume of the ablation zone was calculated using the following equation:

$$V = \pi\ (Dmax \times Dmin \times Dv)/6\ [12]$$

Ablative Margin Outcomes

The ablative margin at the midpoint of the two electrodes (AMm) and the margin at the electrode path (AMe) were assessed to evaluate the ablative margin around the virtual

https://doi.org/10.3348/kjr.2021.0451

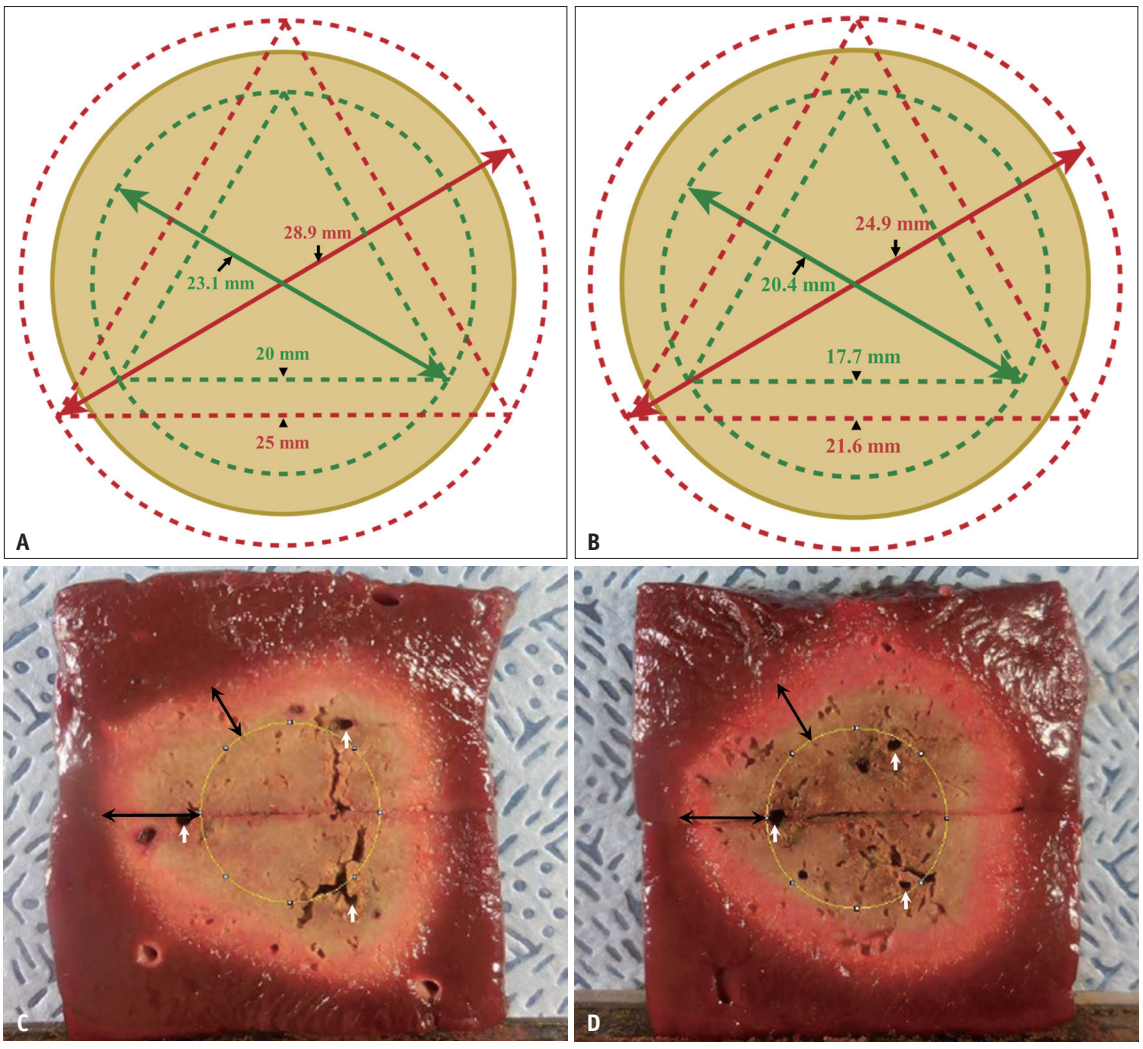

Fig. 3. The calculation method for 25-mm and 20-mm interelectrode distances for no-touch and peripheral tumor-puncturing ablation for a 25-mm virtual tumor.

A. Two equilateral triangles with lengths of 25 mm (red dotted triangle) and 20 mm (green dotted triangle) are drawn on top of each other with the same centroid. These represent the 25-mm and 20-mm interelectrode distances. Circumcircles were drawn passing through the three vertices of these triangles, and their diameters were measured. The diameters of the circumcircles of the 25-mm and 20-mm triangles are measured at 28.9 mm and 23.1 mm, respectively (average diameter of 26.0 mm). Thus, a 25-mm circle (size of a virtual tumor; yellow circle) would be located between the two circles. As the three vertices of the 25-mm triangle are located outside the 25-mm virtual tumor, inserting the electrodes at a 25-mm interelectrode distance would simulate no-touch ablation. As the three vertices of the 20-mm triangle are located within the 25-mm virtual tumor, inserting the electrodes at a 20-mm interelectrode distance would simulate peripheral tumor-puncturing ablation. **B.** After ablation. The interelectrode distance decreases from 25 mm to 21.6 mm (red dotted triangle) and from 20 mm to 17.7 mm (green dotted triangle). Therefore, the calculated contraction rates are 0.864 and 0.885, respectively. Using the abovementioned process, two circumcircles were drawn for the 21.6- and 17.7-mm triangles. The diameters of the two circumcircles were 24.9 mm and 20.4 mm, respectively (average, 22.7 mm). Thus, if the contracted tumor size is between 20.4 and 24.9 mm, its margin would be located inside the three electrodes for no-touch ablation (25-mm interelectrode distance) and outside the three electrodes for peripheral tumor-puncturing ablation (20-mm interelectrode distance). Using the contraction rate, the contracted virtual tumor was estimated to be 21.6 mm for a 25-mm interelectrode distance and 22.1 mm for a 20-mm inter-electrode distance. **C.** Evaluating whether the contracted tumor is located within the three electrodes for no-touch ablation (25-mm interelectrode distance). The interelectrode distance after ablation was measured at a distance of 23.6 mm; thus, a contraction rate of 0.944 was calculated. The size of the virtual tumor after ablation was estimated to be 23.6 mm. A yellow circle with a diameter of 23.6 mm was drawn over the transverse cut plane of the ablation zone. The contracted virtual tumor fits well within the three electrode tracts (white arrows), which is well-suited for no-touch ablation. Peritumoral ablative margins were estimated from the margin of the virtual tumor (yellow circle) to the closest outer margin of the ablation zone (double black arrows). **D.** Evaluating whether the contracted tumor is located outside the three electrodes for peripheral tumor-puncturing ablation (20-mm interelectrode distance). The interelectrode distance after ablation was 18.0 mm; thus, a contraction rate of 0.900 was calculated. The size of the virtual tumor after ablation was estimated to be 22.5 mm. The yellow circle with a diameter of 22.5 mm, representing the contracted virtual tumor, was drawn over the transverse cut plane of the ablation zone. The contracted virtual tumor is located just outside the three electrode tracts (white arrows), which is well suited for peripheral tumor-puncturing ablation. Peritumoral ablative margins were estimated from the margin of the virtual tumor (yellow circle) to the closest outer margin of the ablation zone (double black arrows).

https://doi.org/10.3348/kjr.2021.0451

Korean Journal of Radiology
KJR

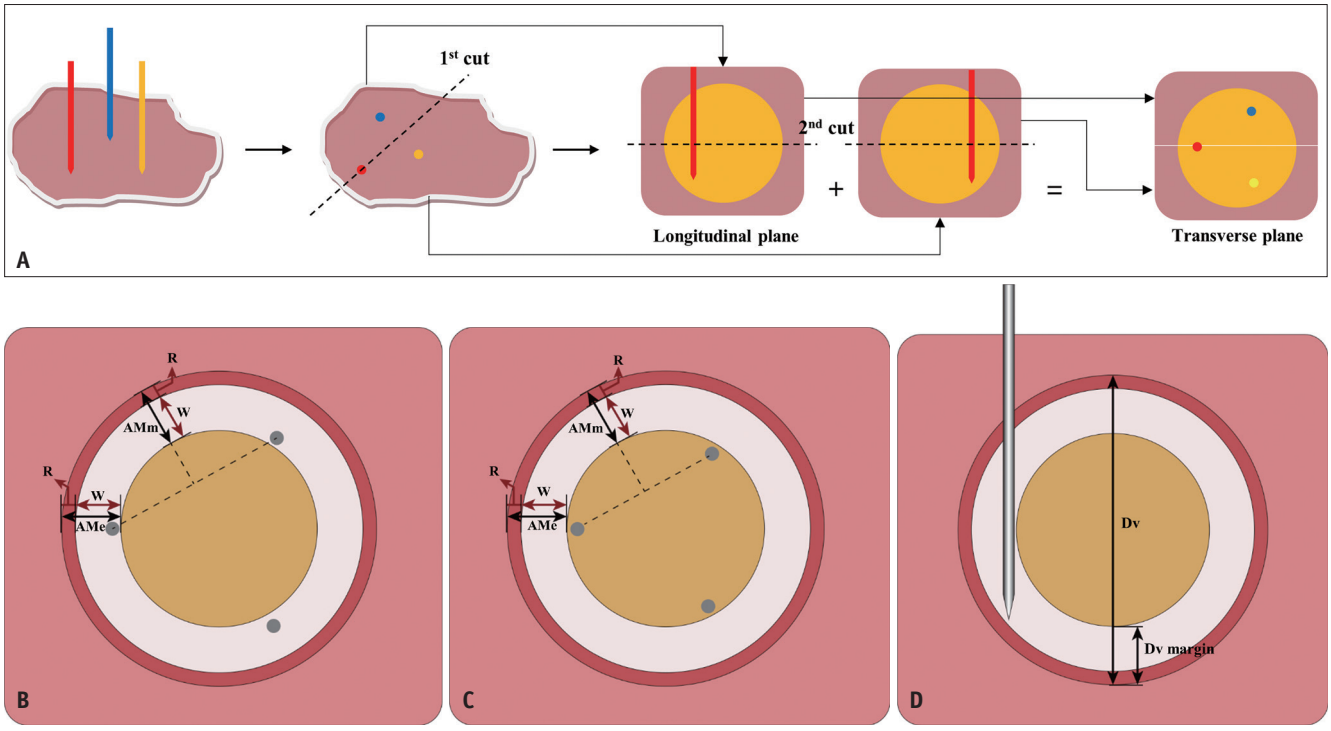

Fig. 4. Schematic showing the surface of the ablation zone.
A. Figure showing how the ablation zone was cut. After ablation, the bovine liver blocks were cut parallel to the electrode tracts. This longitudinal cut surface included one of the electrode tracts and the midline between the other two electrodes. Thereafter, a second cut was made in a transverse plane perpendicular to the electrode tracks so that the cut surface would traverse the center of the ablation zone. The second cut transverse plane shows the interaction between the three electrodes. **B.** Figure showing the transverse plane of the ablation zone at 25-mm interelectrode distance. Note that the electrode paths (small black circles) are located outside the 2.5-cm virtual tumor (yellow circle), representing no-touch ablation. The ablation zone consists of an inner white zone (white area) and an outer red zone (red area). To evaluate the ablative margin around the virtual tumor, the distance between the margin of the virtual tumor at the midpoint of the two electrodes and the closest outer margin of the ablation zone (AMm), and the distance between the margin of the virtual tumor where the electrode was placed and the closest outer margin of the ablation zone (AMe), were assessed. The thicknesses of the red (R) and white (W) zones were evaluated for AMm and AMe. The white zone proportion (the proportion of the white zone at AMm or AMe) was calculated. The Dmax and Dmin diameters were also measured. Circularity was measured by drawing a region of interest along the outer margin of the ablation zone. **C.** Figure showing the transverse plane of the ablation zone at a 20-mm interelectrode distance. Note that the electrode paths (small black circles) are located within the 2.5-cm virtual tumor (yellow circle), representing peripheral tumor-puncturing ablation. The same parameters were evaluated at a distance of 25 mm. **D.** Figure showing the longitudinal plane of the first cut surface. The longitudinal Dv and the margins were measured. The inner yellow circle represents a virtual tumor. The longest Dv parallel to the electrode path was measured in the longitudinal plane. The margin of Dv was also measured. The white-colored area outside the virtual tumor represents a white ablation zone. The outer red area represents the red-ablation zone. AMe = ablative margin at electrode path, AMm = ablative margin at midpoint, Dmax = maximum diameter, Dmin = minimum diameter, Dv = vertical diameter

tumor (Fig. 4B, C). The measurements were performed after drawing a virtual contracted tumor over the transverse plane of each ablation zone, based on the estimated contracted tumor (Fig. 3B-D). AMm is the distance between the margin of the virtual tumor and the closest outer margin of the ablation zone at the midpoint of the two electrodes. It is the most remote site from the electrodes and may have the smallest peritumoral ablative margin. AMe is the distance between the margin of the virtual tumor, where the electrode is placed, and the closest outer margin of the ablation zone. AMe may have the greatest ablative margin because it is the closest to the electrodes.

Moreover, as the ablation zone was composed of the peripheral red zone and central white zone, their thicknesses was measured at AMm and AMe, respectively. Subsequently, the white zone proportion—the proportion of the white zone at AMm or AMe—was calculated.

Sample Size Calculation

A pilot study was performed to estimate the sample size needed to compare ablation zone characteristics among the three protocols. For sample size estimation, it was hypothesized that the circularity, AMe, or AMm would be different among the three energy modes per interelectrode

https://doi.org/10.3348/kjr.2021.0451

distance (20 and 25 mm). In the pilot study, 12 ablation zones were created for each energy mode and for each interelectrode distance. Thus, 72 ablation zones were created for the pilot study. To test the hypotheses at the 5% significance level at each inter-electrode distance, each hypothesis (circularity, AMe, or AMm would be different) was tested by one-way analysis of variance (ANOVA) at a significance level of 0.017 (0.05/3). Considering an effect size of 0.5 (thus, a difference of at least 0.5 x the standard deviation is regarded as clinically significant), it was calculated that 19 ablation zones would be needed for each energy mode at each interelectrode distance to obtain 80% power. Considering a dropout rate of 10%, 22 ablation zones were required for each energy mode. Thus, 66 ablation zones were needed for each interelectrode distance, and a total of 132 ablation zones were created for the main study.

Statistical Analysis

ANOVA or Kruskal–Wallis tests were performed for quantitative variables, according to the data distribution to compare the ablation outcomes among the three ablation energy modes at a given interelectrode distance. If the results of the global test among the three groups were significant, Tukey's test was used for pairwise comparisons when the data were normally distributed; conversely, Tukey's test was applied after rank transformation for non-normally distributed variables. *p* values were corrected by Bonferroni's method for multiple primary endpoints, and values less than 0.05, were considered significant. Statistical analysis was performed using SAS version 9.4 (SAS Institute Inc.).

RESULTS

General Outcomes of RFA

The general outcomes of the RFA are shown in Table 1. The contraction rate ranged from 0.772 to 0.944 at a 25-mm interelectrode distance, and from 0.745 to 0.945 at a 20-mm distance. These rates were not significantly different among the three energy modes at either of the two distances ($p = 0.085$ for 25-mm distance and $p = 0.174$ for 20-mm distance). Likewise, the actual interelectrode distances after ablation and the contracted virtual tumor size among the three energy modes were not significantly different at either of the two distances ($p = 0.085$ for 25-mm distance and $p = 0.174$ for 20-mm distance).

The circularity of the ablation zone was in the following order: SB > DSM + SB > DSM, and it was significantly different among the three energy groups at both distances ($p < 0.001$ and $p = 0.002$ for 25-mm and 20-mm, respectively). In pairwise comparisons, only the circularity of SB was significantly higher than that of DSM ($p < 0.001$), whereas it was significantly different in other comparisons (DSM + SB vs. DSM, $p = 0.159$; and SB vs. DSM + SB, $p = 0.205$) at the 25-mm interelectrode distance. At the 20-mm interelectrode distance, the circularity of SB was higher than that of DSM ($p = 0.003$), and SB was also higher than that of DSM + SB ($p = 0.017$) (Fig. 5).

The total energy delivered was high in the following order: DSM > DSM + SB > SB; it was significantly different among the three energy modes at both distances and between each energy mode in the pairwise comparisons (all $p < 0.001$).

Size Outcomes of RFA

The size outcomes of the RFA are shown in Table 2. All size measurements, including Dmax, Dmin, Dv, and ablation volume, were in the following order at both interelectrode distances: DSM > DSM + SB > SB (all statistically significant). In pairwise comparisons, all size outcomes were significantly different among the three energy modes at both distances, except for Dv. For Dv, only DSM was significantly higher than SB ($p = 0.017$) at a 25-mm distance. Dv with DSM was significantly higher than that with SB ($p < 0.001$) and DSM + SB than SB ($p < 0.001$) at a 20-mm distance.

Ablative Margin Outcomes

The ablative margin outcomes after RFA are shown in Table 3. Similar to the size measurements, AMm and AMe were as follows: DSM > DSM + SB > SB, and the differences were significant among the three energy modes at both interelectrode distances (all $p < 0.001$). The differences were also significant among the three energy modes in pairwise comparisons at both distances.

The white zone thickness at AMm at a 20-mm interelectrode distance was as follows: DSM > DSM + SB > SB, with a significant difference ($p < 0.001$). However, at a 25-mm distance, there was no significant difference among the three energy modes ($p = 0.353$). Meanwhile, the white zone proportion of AMm at a 25-mm distance was different from most other measurements and was as follows: SB > DSM + SB > DSM, with a significant difference ($p = 0.002$). In pairwise comparisons, there were statistically significant

https://doi.org/10.3348/kjr.2021.0451

Korean Journal of Radiology
KJR

differences between SB and DSM (p = 0.005) and between DSM + SB and DSM (p = 0.007), but not between SB and DSM + SB (p = 0.993). At a 20-mm distance, the AMm white zone proportion was not significantly different among the three energy modes (p = 0.066).

For AMe, the white zone thickness was as follows: DSM > DSM + SB > SB (all p < 0.001). These values were also significantly different among the three energy modes in the pairwise comparisons (all statistically significant). However, the white zone proportion at AMe was not significantly different among the three energy modes at both distances (p = 0.090 for 25-mm distance and p = 0.054 for 20-mm distance).

The Dv margin at the 20-mm distance had the same order

Table 1. General Outcomes of Radiofrequency Ablation Under DSM, SB, and Combined DSM + SB Energy Modes at 25-mm and 20-mm Interelectrode Distances

Measurements	Values	Comparison among Energy Modes		
		Overall	Pairwise Comparisons	
		P	Pair	*P**
Actual interelectrode distance, cm				
25-mm		0.085		
1: DSM	2.16 (1.98–2.36)			
2: SB	2.08 (2.00–2.36)			
3: DSM + SB	2.10 (1.93–2.32)			
20-mm		0.174		
4: DSM	1.71 ± 0.07			
5: SB	1.75 ± 0.09			
6: DSM + SB	1.72 ± 0.09			
Contracted virtual tumor, cm				
25-mm		0.085		
1: DSM	2.16 (1.98–2.36)			
2: SB	2.08 (2.00–2.36)			
3: DSM + SB	2.10 (1.93–2.32)			
20-mm		0.174		
4: DSM	2.13 ± 0.09			
5: SB	2.19 ± 0.11			
6: DSM + SB	2.15 ± 0.11			
Circularity				
25-mm		< 0.001		
1: DSM	0.925 ± 0.021		1 vs. 2	< 0.001
2: SB	0.950 ± 0.014		1 vs. 3	0.157
3: DSM + SB	0.938 ± 0.017		2 vs. 3	0.205
20-mm		0.002		
4: DSM	0.960 ± 0.010		4 vs. 5	0.003
5: SB	0.970 ± 0.008		4 vs. 6	> 0.999
6: DSM + SB	0.962 ± 0.008		5 vs. 6	0.017
Energy, Kcal				
25-mm		< 0.001		
1: DSM	13.18 (10.27–15.37)		1 vs. 2	< 0.001
2: SB	7.12 (5.78–7.81)		1 vs. 3	< 0.001
3: DSM + SB	9.99 (8.95–11.61)		2 vs. 3	< 0.001
20-mm		< 0.001		
4: DSM	12.64 (10.16–14.83)		4 vs. 5	< 0.001
5: SB	6.28 (4.95–7.37)		4 vs. 6	< 0.001
6: DSM + SB	9.41 (7.78–11.55)		5 vs. 6	< 0.001

Data are median (range) or mean ± standard deviation. *p < 0.05, considered significant. DSM = dual-switching monopolar, DSM + SB = combined DSM + SB, SB = switching bipolar

https://doi.org/10.3348/kjr.2021.0451

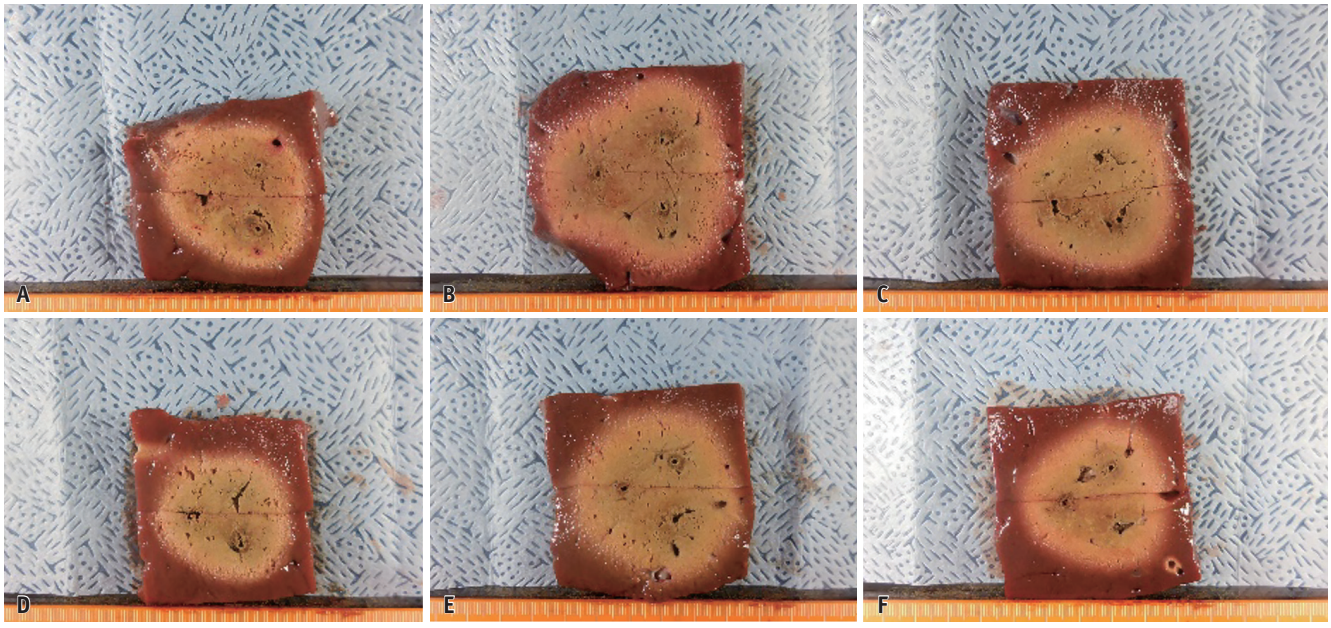

Fig. 5. The bovine liver blocks showing transverse planes ablated under SB, DSM, and combined DSM + SB energy modes at 25-mm (A-C) and 20-mm (D-F) interelectrode distance to ablate a 2.5-cm virtual tumor.
A-C. Radiofrequency ablation zones at 25-mm interelectrode distance under SB **(A)**, DSM **(B)**, and combined DSM + SB **(C)** energy modes. **(A)** The ablation zone with the SB mode was more circular than that with the other energy modes ($p < 0.001$). **(B)** The DSM created a larger ablation zone than the SB ($p < 0.001$), but the ablation zone was less circular. **(C)** The combined DSM + SB seem to fall between the DSM + SB modes. **D-F.** Radiofrequency ablation zones at 20-mm interelectrode distance under SB **(D)**, DSM **(E)**, and combined DSM + SB **(F)** energy modes. The size of the ablation zone was the greatest with DSM mode, followed by that with combined DSM + SB modes, and the smallest with SB mode ($p < 0.001$). Although statistical comparison showed a significant difference in the ablation zone circularity among the energy modes ($p = 0.002$), all three energy modes seemed to create a circular ablation zone at a 20-mm interelectrode distance (circularity: 0.960 for DSM, 0.970 for SB, and 0.962 for combined DSM + SB). DSM = dual switching monopolar, DSM + SB = combined DSM + SB, SB = switching bipolar

as most measurements (DSM > DSM + SB > SB), with a significant difference ($p < 0.001$); however, at the 25-mm distance, the values were not significantly different among the three energy modes ($p = 0.079$).

DISCUSSION

In the present study, we compared three energy modes (DSM, SB, and DSM + SB) in the simulation of a 25-mm tumor ablation at 25-mm and 20-mm interelectrode distances. The 25-mm interelectrode distance represented no-touch ablation, while the 20-mm distance represented peripheral tumor-puncturing ablation. The total procedure time for each energy protocol was 5 minutes, which may be comparable to that of microwave ablation.

The greatest circularity was achieved with the SB mode at both interelectrode distances. The ablation zone size and ablative margins were the largest in the DSM mode, followed by the DSM + SB and SB modes. However, the white zone proportion, in general, was highest in the SB mode, followed by the DSM + SB and DSM modes.

The circularity of the ablation zone was analyzed in our study since a circle can uniformly cover the tumor and peritumoral liver parenchyma in all directions, especially for small tumors that are usually round or spherical [13]. The highest circularity was achieved with the SB mode, which was significantly higher than that with the DSM mode at both the distances. The circularity of the three energy modes was high at a 20-mm interelectrode distance (all values > 0.960), however, it was relatively low for DSM (0.925) at a 25-mm distance. These results may imply that all ablation zones are circular at a 20-mm interelectrode distance, despite the statistically significant differences among the three energy modes. However, at a 25-mm interelectrode distance, the DSM mode achieved relatively less circularity of the ablation zone, while it increased when DSM was combined with the SB mode.

In terms of the size of the ablation zone, all measurements were in the order of DSM > DSM + SB > SB. This outcome is expected because energy is radiated centrifugally from each electrode in the monopolar mode, and the ablation zones from each electrode are merged to create the final ablation zone. In contrast, the energy flow between the electrodes in the bipolar mode and the energy

https://doi.org/10.3348/kjr.2021.0451

Korean Journal of Radiology
KJR

Table 2. Size Outcomes of Radiofrequency Ablation Under DSM, SB, and Combined DSM + SB Energy Modes at 25-mm and 20-mm Interelectrode Distances

Measurements	Values	Comparison among Energy Modes		
		Overall	Pairwise Comparisons	
		P	Pair	*P**
Dmax, cm				
25-mm		< 0.001		
1: DSM	5.10 ± 0.21		1 vs. 2	< 0.001
2: SB	4.37 ± 0.16		1 vs. 3	< 0.001
3: DSM + SB	4.74 ± 0.20		2 vs. 3	< 0.001
20-mm		< 0.001		
4: DSM	4.86 ± 0.28		4 vs. 5	< 0.001
5: SB	4.11 ± 0.21		4 vs. 6	< 0.001
6: DSM + SB	4.51 ± 0.30		5 vs. 6	< 0.001
Dmin, cm				
25-mm		< 0.001		
1: DSM	4.92 (4.61–5.28)		1 vs. 2	< 0.001
2: SB	4.20 (4.03–4.67)		1 vs. 3	< 0.001
3: DSM + SB	4.55 (4.27–4.85)		2 vs. 3	< 0.001
20-mm		< 0.001		
4: DSM	4.70 ± 0.24		4 vs. 5	< 0.001
5: SB	3.93 ± 0.20		4 vs. 6	< 0.001
6: DSM + SB	4.34 ± 0.27		5 vs. 6	< 0.001
Dv, cm				
25-mm		0.022		
1: DSM	4.17 ± 0.24		1 vs. 2	0.017
2: SB	4.00 ± 0.18		1 vs. 3	0.248
3: DSM + SB	4.07 ± 0.18		2 vs. 3	0.442
20-mm		< 0.001		
4: DSM	4.24 (3.95–4.52)		4 vs. 5	< 0.001
5: SB	3.84 (3.64–4.19)		4 vs. 6	0.207
6: DSM + SB	4.11 (3.49–4.67)		5 vs. 6	< 0.001
Volume, cm^3				
25-mm		< 0.001		
1: DSM	54.68 (42.76–69.61)		1 vs. 2	< 0.001
2: SB	38.20 (34.13–45.80)		1 vs. 3	< 0.001
3: DSM + SB	46.44 (38.72–55.20)		2 vs. 3	< 0.001
20-mm		< 0.001		
4: DSM	50.78 ± 6.92		4 vs. 5	< 0.001
5: SB	32.78 ± 4.18		4 vs. 6	< 0.001
6: DSM + SB	42.76 ± 8.21		5 vs. 6	< 0.001

Data are median (range) or mean ± standard deviation. *p < 0.05, considered significant. DSM = dual-switching monopolar, DSM + SB = combined DSM + SB, SB = switching bipolar

concentrated between the electrodes creates an ablation zone mainly between the electrodes. Therefore, compared with the monopolar mode, there is less expansion of the ablation zone in the bipolar mode, resulting in a smaller ablation zone.

In our study, the ablative margins around the virtual tumor were evaluated at two points, AMm and AMe. AMm is the crossing point of the two energies radiated from each electrode in the monopolar mode. Therefore, it could be considered the most vulnerable point where a sufficient peritumoral ablative margin may not be achieved if there is insufficient confluence of the ablation zones created by each electrode. AMm may also be a vulnerable point in the bipolar mode since it would be the ablation zone with a

 https://doi.org/10.3348/kjr.2021.0451

Table 3. Ablative Margin Outcomes After Radiofrequency Ablation Under DSM, SB, and Combined DSM + SB Energy Modes at 25-mm and 20-mm Interelectrode Distances

Measurements	Values	Comparison among Energy Modes		
		Overall	Pairwise Comparisons	
		P	Pair	*P**
AMm, cm				
25-mm		< 0.001		
1: DSM	1.06 ± 0.15		1 vs. 2	< 0.001
2: SB	0.84 ± 0.09		1 vs. 3	0.028
3: DSM + SB	0.95 ± 0.12		2 vs. 3	0.047
20-mm		< 0.001		
4: DSM	1.11 (0.94–1.48)		4 vs. 5	< 0.001
5: SB	0.76 (0.54–0.96)		4 vs. 6	< 0.001
6: DSM + SB	0.94 (0.71–1.24)		5 vs. 6	< 0.001
AMm white zone, cm				
25-mm		0.353		
1: DSM	0.46 ± 0.15			
2: SB	0.43 ± 0.10			
3: DSM + SB	0.48 ± 0.12			
20-mm		< 0.001		
4: DSM	0.55 ± 0.11		4 vs. 5	< 0.001
5: SB	0.33 ± 0.11		4 vs. 6	0.002
6: DSM + SB	0.44 ± 0.09		5 vs. 6	0.003
AMm white zone proportion, %				
25-mm		0.002		
1: DSM	42.55 ± 8.70		1 vs. 2	0.005
2: SB	50.62 ± 8.29		1 vs. 3	0.007
3: DSM + SB	50.33 ± 7.37		2 vs. 3	0.993
20-mm		0.066		
4: DSM	48.54 (38.35–55.39)			
5: SB	42.46 (26.97–60.25)			
6: DSM + SB	46.16 (33.97–53.09)			
AMe, cm				
25-mm		< 0.001		
1: DSM	1.67 ± 0.12		1 vs. 2	< 0.001
2: SB	1.23 ± 0.11		1 vs. 3	< 0.001
3: DSM + SB	1.44 ± 0.12		2 vs. 3	< 0.001
20-mm		< 0.001		
4: DSM	1.43 (1.27–1.75)		4 vs. 5	< 0.001
5: SB	0.96 (0.83–1.26)		4 vs. 6	< 0.001
6: DSM + SB	1.20 (1.02–1.62)		5 vs. 6	< 0.001
AMe white zone, cm				
25-mm		< 0.001		
1: DSM	1.18 ± 0.11		1 vs. 2	< 0.001
2: SB	0.90 ± 0.09		1 vs. 3	< 0.001
3: DSM + SB	1.04 ± 0.11		2 vs. 3	< 0.001
20-mm		< 0.001		
4: DSM	0.94 (0.73–1.13)		4 vs. 5	< 0.001
5: SB	0.59 (0.50–0.94)		4 vs. 6	< 0.001
6: DSM + SB	0.75 (0.54–1.04)		5 vs. 6	< 0.001

https://doi.org/10.3348/kjr.2021.0451

Korean Journal of Radiology
KJR

Table 3. Ablative Margin Outcomes After Radiofrequency Ablation Under DSM, SB, and Combined DSM + SB Energy Modes at 25-mm and 20-mm Interelectrode Distances (Continued)

Measurements	Values	Comparison among Energy Modes		
		Overall	Pairwise Comparisons	
		P	Pair	*P**
AMe white zone proportion, %				
25-mm		0.090		
1: DSM	70.90 ± 3.08			
2: SB	73.04 ± 2.81			
3: DSM + SB	71.91 ± 3.57			
20-mm		0.054		
4: DSM	64.43 ± 3.63			
5: SB	64.66 ± 4.40			
6: DSM + SB	62.05 ± 3.55			
Dv margin, cm				
25-mm		0.079		
1: DSM	0.96 (0.67–1.26)			
2: SB	0.88 (0.73–1.19)			
3: DSM + SB	0.93 (0.77–1.12)			
20-mm		< 0.001		
4: DSM	1.03 (0.88–1.43)		4 vs. 5	< 0.001
5: SB	0.76 (0.60–1.05)		4 vs. 6	0.527
6: DSM + SB	1.02 (0.69–1.32)		5 vs. 6	< 0.001

Data are median (range) or mean ± standard deviation. *$p < 0.05$, considered significant. AMe = ablative margin at electrode path, AMm = ablative margin at the midpoint of two electrodes, DSM = dual-switching monopolar, DSM + SB = combined DSM + SB, Dv = longest vertical diameter parallel to the electrode paths on the longitudinal plane, SB = switching bipolar

short diameter if the ablation zone was ovoid instead of circular.

In our study, the energy modes of RFA affected the ratio of the central white zone and peripheral red zone, both of which constituted the ablation zone. The white zone proportion of AMm at a 25-mm interelectrode distance was the lowest in the DSM mode, although the ablative margin with DSM was the largest when compared with that in the other energy modes. A previous study demonstrated that the central white zone corresponded to total necrosis, whereas the peripheral red zone was a mixture of dying and dead cells [14]. Although it is unknown which of the two zones (white zone only or white + red zone) should be considered in the evaluation of the true ablation zone, a larger white zone would be preferable to ensure complete tumor necrosis. Therefore, the DSM mode alone may not effectively achieve an adequate ablative margin at the midpoint between the two electrodes owing to the relatively thick red zone. Instead, the SB mode would be more efficient in eradicating actual tumor cells.

Meanwhile, the AMe seems sufficient for all energy modes at both interelectrode distances, except for SB at the 20-mm interelectrode distance (AMe: 0.96 cm), when the targeted ablative margin is > 1 cm. Therefore, as with AMm, DSM may be needed to obtain a sufficient ablative margin (AMe under DSM + SB: 1.44 cm at 25-mm distance and 1.20 cm at 20-mm distance). However, the DSM mode may only create excessive AMe at both distances, especially at the 25-mm interelectrode distance (1.67 cm).

Our results may provide practical tips for RFA with multiple electrodes because peripheral tumor puncturing can occur unintentionally. If the tumor is punctured in the periphery, the SB mode may not create a sufficient ablative margin. In this case, the DSM mode is required to achieve an adequate ablative margin. Nevertheless, ablation with the SB mode may be performed to ensure complete tumor necrosis. When the no-touch needle placement is successfully executed, the DSM + SB or SB modes would be valuable for avoiding excessive ablative margins.

This study has several limitations. First, this was an *ex vivo* study, and the results obtained were not verified *in vivo*. The shape of the ablation zone *in vivo* may not be as round as that observed *ex vivo*, as shown in a previous study in the DSM energy mode [10,15]. Nevertheless, our

 https://doi.org/10.3348/kjr.2021.0451

results provide background information on the ablation performance of various energy modes, especially DSM + SB, at 25-mm and 20-mm interelectrode distances using three separable clustered electrodes. Further tests, including *in vivo* experiments, are required to verify our results. Second, ablations were performed in the hepatic parenchyma without actual tumors. The ablative margins were measured by drawing a virtual tumor based on mathematical calculations, since bovine models of liver cancer are difficult to generate. Liver cancer models in small animals, such as mice, cannot be employed owing to the small liver sizes. Implanting tumor mimickers made of a mixture of agarose, cellulose, glycerol, and methylene blue [16] could have been considered, but the shape and size of the mimickers may not have been uniform, complicating the measurements for peritumoral margins. Third, only visual inspection was performed without histologic analysis to evaluate the ablation zones. However, as mentioned earlier, the central white zone corresponded to total necrosis, whereas the peripheral red zone corresponded to a mixture of dying and dead cells [14]. Therefore, our approach was not expected to significantly limit the study results.

In conclusion, circularity was the greatest in the SB mode and lowest in the DSM mode. The DSM mode produced a larger ablation zone and peritumoral ablative margin than the other energy modes, while ablation in the SB mode achieved more complete necrosis. Therefore, the DSM and SB modes appear complementary in creating an ideal ablation zone. Bipolar ablation is needed to efficiently eradicate tumors and create a circular ablation zone, while monopolar ablation is required to create a sufficient ablative margin and a large ablation zone.

Availability of Data and Material

The datasets generated or analyzed during the study are available from the corresponding author on reasonable request.

Conflicts of Interest

Technical support was provided from Starmed Co., Ltd. (Korea). However, only the authors from Samsung Medical Center had full control of the study design, data collection, analysis and interpretation, decision to publish, and preparation of the manuscript.
Min Woo Lee who is on the editorial board of the *Korean Journal of Radiology* was not involved in the editorial evaluation or decision to publish this article. All remaining authors have declared no conflicts of interest.

Author Contributions

Conceptualization: Dong Ik Cha, Min Woo Lee, Seong Eun Ko, Hyunchul Rhim. Data curation: Dong Ik Cha, Min Woo Lee. Formal analysis: Dong Ik Cha, Min Woo Lee, Kyoung Doo Song. Funding acquisition: Dong Ik Cha, Min Woo Lee. Investigation: Dong Ik Cha, Min Woo Lee. Methodology: Dong Ik Cha, Min Woo Lee. Supervision: Min Woo Lee. Writing—original draft: Dong Ik Cha, Min Woo. Writing—review & editing: all authors.

ORCID iDs

Dong Ik Cha
https://orcid.org/0000-0003-3271-6532
Min Woo Lee
https://orcid.org/0000-0001-9048-9011
Kyoung Doo Song
https://orcid.org/0000-0002-2767-3622
Seong Eun Ko
https://orcid.org/0000-0003-0007-6569
Hyunchul Rhim
https://orcid.org/0000-0002-9737-0248

Funding Statement

This study has received a research fund from Samsung Medical Center (SMX1200871).

REFERENCES

1. Ahmed M, Brace CL, Lee FT Jr, Goldberg SN. Principles of and advances in percutaneous ablation. *Radiology* 2011;258:351-369
2. Ahmed M, Solbiati L, Brace CL, Breen DJ, Callstrom MR, Charboneau JW, et al. Image-guided tumor ablation: standardization of terminology and reporting criteria--a 10-year update. *Radiology* 2014;273:241-260
3. Dodd GD 3rd, Frank MS, Aribandi M, Chopra S, Chintapalli KN. Radiofrequency thermal ablation: computer analysis of the size of the thermal injury created by overlapping ablations. *AJR Am J Roentgenol* 2001;177:777-782
4. Park MJ, Kim YS, Rhim H, Lim HK, Lee MW, Choi D. A comparison of US-guided percutaneous radiofrequency ablation of medium-sized hepatocellular carcinoma with a cluster electrode or a single electrode with a multiple overlapping ablation technique. *J Vasc Interv Radiol* 2011;22:771-779
5. Kim YS, Lim HK, Rhim H, Lee MW, Choi D, Lee WJ, et al. Ten-year outcomes of percutaneous radiofrequency ablation as

https://doi.org/10.3348/kjr.2021.0451

first-line therapy of early hepatocellular carcinoma: analysis of prognostic factors. *J Hepatol* 2013;58:89-97
6. Seror O, N'Kontchou G, Van Nhieu JT, Rabahi Y, Nahon P, Laurent A, et al. Histopathologic comparison of monopolar versus no-touch multipolar radiofrequency ablation to treat hepatocellular carcinoma within Milan criteria. *J Vasc Interv Radiol* 2014;25:599-607
7. Hocquelet A, Aubé C, Rode A, Cartier V, Sutter O, Manichon AF, et al. Comparison of no-touch multi-bipolar vs. monopolar radiofrequency ablation for small HCC. *J Hepatol* 2017;66:67-74
8. Seror O, N'Kontchou G, Nault JC, Rabahi Y, Nahon P, Ganne-Carrié N, et al. Hepatocellular carcinoma within Milan criteria: no-touch multibipolar radiofrequency ablation for treatment-long-term results. *Radiology* 2016;280:611-621
9. Yoon JH, Lee JM, Woo S, Hwang EJ, Hwang I, Choi W, et al. Switching bipolar hepatic radiofrequency ablation using internally cooled wet electrodes: comparison with consecutive monopolar and switching monopolar modes. *Br J Radiol* 2015;88:20140468
10. Yoon JH, Lee JM, Han JK, Choi BI. Dual switching monopolar radiofrequency ablation using a separable clustered electrode: comparison with consecutive and switching monopolar modes in ex vivo bovine livers. *Korean J Radiol* 2013;14:403-411
11. Lee DH, Lee MW, Kim PN, Lee YJ, Park HS, Lee JM. Outcome of no-touch radiofrequency ablation for small hepatocellular carcinoma: a multicenter clinical trial. *Radiology* 2021;301:229-236
12. Cha DI, Lee MW, Jeong WK, Ha SY, Ahn SH, Rhim H, et al. Comparison of ablation performance between dual internally cooled wet tip and conventional dual internally cooled tip radiofrequency electrodes: an experimental study in ex vivo bovine liver. *Int J Hyperthermia* 2021;38:332-340
13. Federle MP, Lau J. *Imaging in abdominal surgery*. Philadelphia: Elsevier Health Sciences, 2019
14. Song KD, Lee MW, Rhim H, Kang TW, Cha DI, Yang J. Chronological changes of radiofrequency ablation zone in rabbit liver: an in vivo correlation between gross pathology and histopathology. *Br J Radiol* 2017;90:20160361
15. Yoon JH, Lee JM, Hwang EJ, Hwang IP, Baek J, Han JK, et al. Monopolar radiofrequency ablation using a dual-switching system and a separable clustered electrode: evaluation of the in vivo efficiency. *Korean J Radiol* 2014;15:235-244
16. Scott DJ MD, Young WN, Watumull LM, Lindberg G, Fleming JB, Rege RV, et al. Development of an in vivo tumor-mimic model for learning radiofrequency ablation. *J Gastrointest Surg* 2000;4:620-625

 https://doi.org/10.3348/kjr.2021.0451